HAL
open science

Nano-beam clamping revisited

Ilya Golokolenov, Sumit Kumar, Baptiste Alperin, Bruno Fernandez, Andrew Fefferman, Eddy Collin

To cite this version:

Ilya Golokolenov, Sumit Kumar, Baptiste Alperin, Bruno Fernandez, Andrew Fefferman, et al.. Nano-beam clamping revisited. Journal of Applied Physics, 2023, 133 (12), pp.124302. 10.1063/5.0137869 . hal-04053758

HAL Id: hal-04053758

https://hal.science/hal-04053758v1

Submitted on 31 Mar 2023

HAL is a multi-disciplinary open access archive for the deposit and dissemination of scientific research documents, whether they are published or not. The documents may come from teaching and research institutions in France or abroad, or from public or private research centers.

L'archive ouverte pluridisciplinaire **HAL**, est destinée au dépôt et à la diffusion de documents scientifiques de niveau recherche, publiés ou non, émanant des établissements d'enseignement et de recherche français ou étrangers, des laboratoires publics ou privés.

Nano-beam clamping revisited

Ilya Golokolenov,[†] Sumit Kumar,[†,‡] Baptiste Alperin,[†] Bruno Fernandez,[†]
Andrew Fefferman,[†] and Eddy Collin[*,†]

†*Univ. Grenoble Alpes, Institut Néel, 25 rue des Martyrs, Grenoble, 38042, France*

‡*Royal Holloway University of London, Egham, Surrey, TW20 0EX, England*

E-mail: eddy.collin@neel.cnrs.fr

Abstract

Within recent years, the field of nano-mechanics has diversified in a variety of applications, ranging from quantum information processing to biological molecules recognition. Among the diversity of devices produced these days, the simplest (but versatile) element remains the *doubly-clamped beam*: it can store very large tensile stresses (producing high resonance frequencies f_0 and quality factors Q), is interfaceable with electric setups (by means of conductive layers), and can be produced easily in clean rooms (with scalable designs including multiplexing). Besides, its mechanical properties are the simplest to describe. Resonance frequencies and Qs are being modeled, with as specific achievement the ultra-high quality resonances based on "soft clamping" and "phonon shields". Here, we demonstrate that the fabrication undercut of the clamping regions of basic nano-beams produces a "natural soft clamping", given for free. We present the analytic theory that enables to fit experimental data, which can be used for $\{Q, f_0\}$ design: beyond Finite Element Modeling validation, the presented expressions provide a profound understanding of the phenomenon, with both a Q enhancement and a downwards frequency shift.

Keywords

Nano-mechanics (NEMS), mode frequency, mode dissipation, soft clamping

Introduction

Doubly-clamped nano-beams are utterly basic, but nonetheless remarkably versatile. They are routinely used in a broad range of applications, from mass sensing[1] to quantum electronics.[2] About two decades ago, it had been found that stoichiometric Silicon-Nitride (Si_3N_4) thin films grown on Silicon can store very large tensile stresses, and that subsequently mechanical nano-structures patterned on this material display very high flexural resonance frequencies f_0, and interestingly *very high Q factors*.[3] This phenomenon has been named "dissipation dilution": it is due to the large stored elastic energy, as compared to the losses which arise from bending.[4,5] Indeed, bending losses have been found experimentally to be essentially stress-independent.[6–8] The precise amount of stress stored in the structures can be tuned by stoichiometry, but also by chip-bending,[4] by the design of the beam shape[9] and by the clamping pillars.[10]

A precise (yet phenomenological) modeling of the flexure of beams had been proposed considering ideal clamping,[11] and then successfully adapted to membranes.[12] It is based on a numerical solution of the *Euler-Bernoulli* equation which describes the low-frequency dynamics of thin-and-long beams,[13] matching the observed Q factor linear increase with beam length L, and decrease with mode number n. The key argument is to assume that internal microscopic friction mechanisms originate from the bending of the material, whatever they might be. In this sense, the model applies as well to pure nitride structures[11] as to bi-material devices where a metallic layer dominates the damping.[8,12,14,15] It also works for both room-temperature[11,12] and low temperature[8] experiments. For the former, it has been argued that losses are dominated by surface effects;[6] for the latter, a specific mechanism based on Two-Level-Systems (TLSs) present in the materials is discussed in the literature.[16–18]

Beyond internal damping, the anchoring points appear to play a very important role in beam dynamics. The vibration of the mechanical modes irradiates acoustic waves in the supports, which limits the Q. This radiation damping has been modeled in particular for thin supports,[19–22] which is typically the geometry obtained when the fabrication process under-etches the clamps (so-called *undercut*). Such structures are very common in the literature, and are the focus of the present manuscript. The actual limiting Q-value depends on the precise geometry of the beam (particularly its width w and length L), and of the anchor. Experimentally, for the first flexure $n = 1$ of millimeter length low-stress structures resonating at sub-MHz frequencies, radiation loss seems irrelevant for widths $w < 3$ μm;[23] for high-stress devices (tens of MHz frequencies) with width $w \sim 200$ nm, acoustic radiation dominates for $L < 10$ μm.[24] This leaves a large playground to experimentalists where bending is the main source of losses.[25] On the other hand, when radiation losses dominate it is possible to suppress them with a clamp structuring that forbids phonon transport at the specific frequency of the mode n that one wants to protect: a so-called "phonon shield".[24,26,27]

But the anchoring does more than enabling irradiation into the bulk: it defines the *precise bending shape* at the clamping point. It had been realized about a decade ago that most of the friction occurs near the beam's ends, where the bending is the most dramatic.[23,28] As such, beyond creating phonon gaps in the substrate's density of states, structuring the clamps has another (more trivial) effect: it can reduce this bending and mitigate the losses, which is named "soft clamping".[26,29,30] In this Letter, we demonstrate experimentally that a clamp undercut acts essentially as a "soft clamping" given for free: the quality factor Q of the flexural modes *grows* with the beam width w, which is the reverse behavior when compared to acoustic radiation. As well, the clamp modifies substantially the resonance frequencies[31] (we show that it *decreases* with w), which can be used for design purposes, for instance for nano-beam resonance multiplexing.[32]

Early beam clamp modeling relied on phenomenological ansatzs.[23,28] Instead, here we present an exact analytic theory which follows the same lines as the modeling performed on

membranes.[12] It is based on a high-stress Taylor expansion of the modal parameters (for any mode n), introducing as fit parameters a mass-loaded spring and torque at each of the beam's ends. We demonstrate that *both* the resonance frequency f_0 and Q can be fit with a *clamp spring coefficient* $\alpha_{l,r}$ (l, r for left and right), the torque being (at lowest order) negligible. $\alpha_{r,l}$ is found to be proportional to frequency and inversely proportional to width w, the prefactor being a characteristic of the anchor's shape (and material) solely. We believe that our results constitute a very useful tool when designing *basic* doubly-clamped beams presenting a characteristic fabrication undercut.

Results

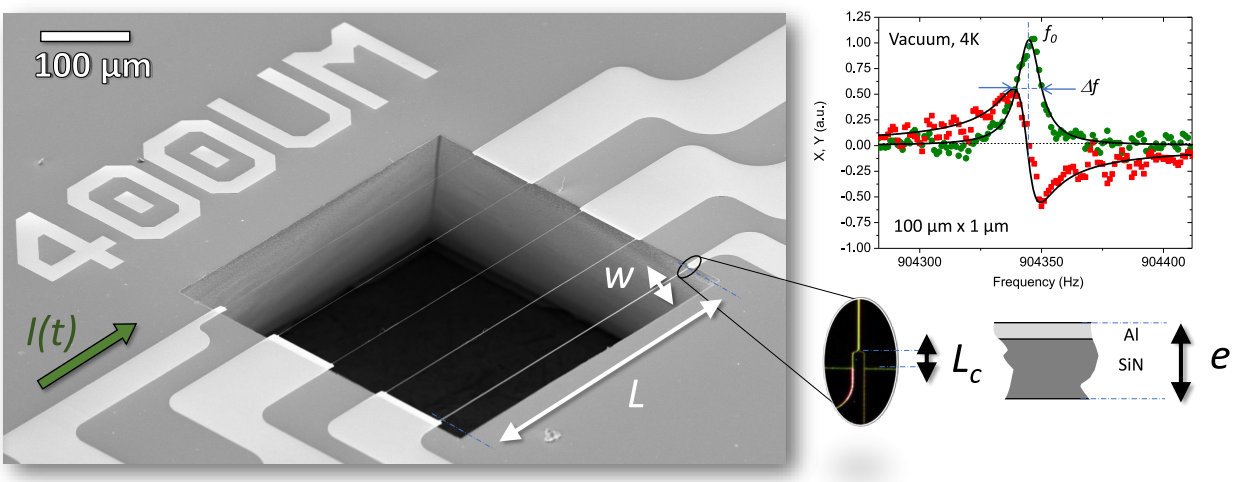

Figure 1: Left: SEM image of one sample (400 μm long beams), with device widths w of 50 nm, 100 nm, 200 nm, 500 nm and 1000 nm (from top to bottom). Bottom-right inset: dark field image of clamping region (suspended part of length L_c), and schematic of the layered structure (not to scale). Top-right: typical phase-resolved linear response line measured for one of our devices (first flexure $n = 1$ of a 100 μm long, 1 μm large one). Drive current I_0 of 0.5 nA, B_0 field 0.2 T. Lines are Lorentzian fits with normalized heights (see text for details).

Experimental details

Nano-beams of various widths and lengths have been realized from low-stress Silicon-Nitride. All have a thickness of about 100 nm, and come from the same wafer. A conductive layer (30 nm Aluminum) has been deposited on top in order to create electrical contacts (total thickness $e = 130$ nm). A typical sample SEM image is shown in Fig. 1 (left), with a zoom-in on one of the clamping regions (inset, with schematic of the bilayer structure). The design is such that the beams are all *fully suspended* within a hollow window; they are connected to the bulk only through a well-defined over-hanging clamp of length L_c (of order 12 μm for all of them). This part has the same thickness (and same constitution) as the rest of the beam, which guarantees that all the layer's stress is transmitted within the structure. The absence of pedestals holding the beams enables to avoid stress-relaxation effects occurring when beams are released, and the pedestals bending.[10] The over-hanging rectangular zone is actually defined through the wet KOH etch: due to the 54.74° angle that the etching creates in the silicon substrate (referenced to the wafer surface), the opening is smaller on the front side than on the back. This generates very straight and clean suspended clamp regions, ideal for a model experiment. It has to be contrasted with usual undercuts linked to the releasing etching time, which are less well-defined.[31] A description of the fabrication process can be found in Ref.[32] Details about sample characteristics can be found in Supplementary Information.

The measurements are performed using the magnetomotive technique.[33] A current $I(t) = I_0 \cos(\omega t + \varphi)$ is fed into the beam which stands in a static magnetic field B_0, thus generating a force $\propto I_0 B_0$ at frequency ω. Used fields typically range from 0.2 T to 1 T, and care is taken to take all data in the linear regime, characterizing carefully the extra damping coming from the electric circuit[33] (which needs to be subtracted). Each sample consists in a set of beams of equal lengths, but with widths ranging from 50 nm to 1000 nm. For a given sample, all beams can be connected in series, which enables a straightforward multiplexing (see Fig. 1). Besides, each beam can also be connected independently, in order to separate

its resonances from other devices without ambiguity. As beams move out-of-plane, a voltage $V(t)$ is induced at their extremities, proportional to field B_0 and velocity. Only symmetric modes are detected, the signal being proportional to the maximal amplitude of motion; anti-symmetric ones cancel out. Measurements are conducted in cryogenic vacuum at 4.2 K, using a lock-in amplifier (with in-phase X and quadrature Y components). An example of resonance peaks obtained via a frequency-sweep is shown in Fig. 1 (right). More details on the setup can be found in Ref.[32]

Data Analysis and Theory

From the measured peaks one extracts resonance frequency f_0 (centre position) and damping Δf (full width at half height on X component), giving us the quality factor $Q = f_0/\Delta f$. This is performed on three different 100 μm long samples, two sets of 300 μm and 400 μm ones, and one set of 200 μm beams. Only on one set (100 μm long, 1 μm wide) did we measure the mode dependence (with $n = 1, 3, 5$). Only very few points have been dropped from the statistics, due we believe to fabrication irreproducibility: the 50 nm beams are not very homogeneous in width, and even break with thermal cycling. On some beams, defects can be seen (which look like some sort of filaments, see Fig. 1), which might not be negligible for the narrowest $w = 100$ nm devices. Besides, we see a similar scatter in measured damping (up to a factor 2) as in Ref.[11] from one sample to the other. The final error bars in our graphs therefore reflect the statistical scatter due to the fabrication process. For details, see Ref.[32] and Supplementary Information.

The starting point of the modeling is the Euler-Bernoulli equation that describes the flexure of long-and-thin beams.[13] As in Ref.[12] we define as small parameter:

$$a = \sqrt{\frac{E\,I_z}{SL^2}}, \tag{1}$$

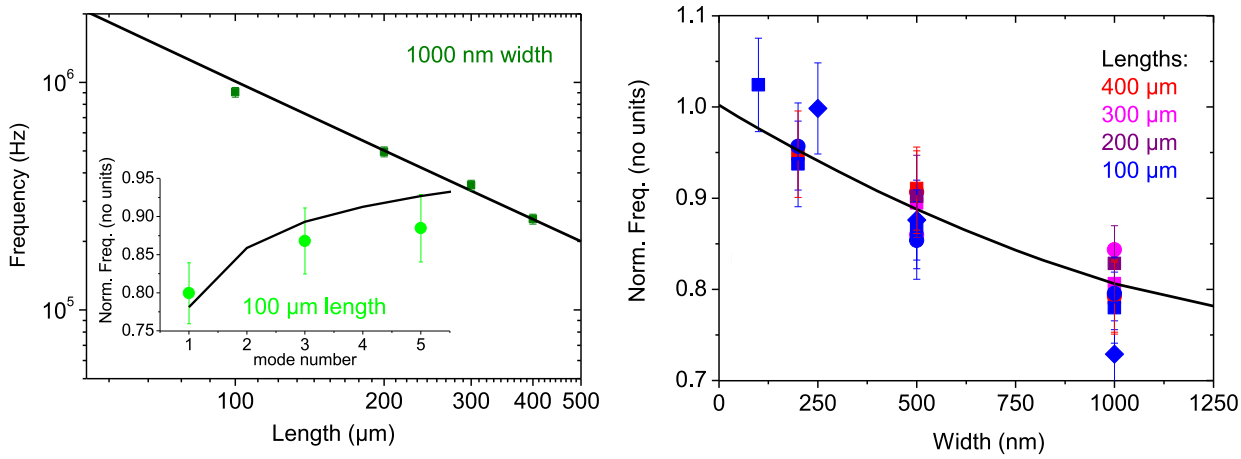

Figure 2: Left, main: dependence of frequency on length L for the first flexure $n = 1$ (all devices having $w = 1000$ nm). Left, inset: frequency of 100 μm long, 1000 nm wide device normalized to the extrapolated value $f_{n,0}$ at $w \to 0$ as a function of mode number n. Right: same normalized frequency for mode $n = 1$ of all devices, as a function of width w. The lines correspond to Eqs. (2,34) with $L = 100$ μm, using a simple ansatz for the clamp parameter α, see text.

with E the Young's modulus and $S = \sigma\, we$ the tensile force acting on the beam (σ is the in-built axial stress). The second moment of area $I_z = \frac{1}{12} we^3$ is a geometrical parameter. The composite nature of the beam can be accounted for by choosing an effective Young's modulus E that depends on the E_{SiN} and E_{Al} of the two materials and on their thickness[34] (and taking for ρ the mean density). In practice, this parameter is close to the E_{SiN} elastic constant, about 200 GPa (± 50 %) from the literature.[10,11] Numerical values for our experiment can be found in Supplementary Information. The specificity of the approach lies in the boundary conditions: on each side (l, r for left and right) we impose an elastic force and an inertial force. They are combined into an *effective spring constant* $k_{l,r} = \frac{S}{L}\alpha_{l,r}$. Similarly, a torque (that combines elastic and inertial contributions) acts also on each end of the beam, resulting in an *effective torsion spring* $\Gamma_{l,r} = SL\,\gamma_{l,r}$. The (dimensionless) constants α_l, γ_l and α_r, γ_r fully characterize each of the l, r clamps, respectively. Ideal clamping is recovered with $\alpha_{l,r}, \gamma_{l,r} \to \infty$, which leads to the conventional boundary conditions (no displacement, no bending angle at both ends). The exact analytical solutions for f_0 and Q are finally derived to second order in a, and $1/\alpha_{l,r}, 1/\gamma_{l,r}$ (the explicit damping model producing Δf is discussed thereafter). We

fit them on data, and find out that $\gamma_{l,r}$ can be to first approximation neglected; besides, only symmetric clamping will be addressed with $\alpha_l = \alpha_r = \alpha$. Nonetheless, the full mathematical description is given in Supplementary Information.

Let us first discuss the resonance frequency parameter f_0 (given here in Hz). For any mode n, it writes:

$$f_0(n, a, \alpha) = f_{n,0}\, P_f(n, a, \alpha), \tag{2}$$

with $2\pi \times f_{n,0} = \frac{n\pi}{L}\sqrt{\frac{\sigma}{\rho}}$ the usual n^{th} resonance frequency of a string (of density ρ), and P_f a correction function. The latter is found to be:

$$\begin{aligned} P_f(n, a, \alpha) &= 1 - \frac{2}{\alpha} + \frac{4}{\alpha^2} \\ &+ a\left(2 - \frac{8}{\alpha} + \frac{2(12 - n^2\pi^2)}{\alpha^2}\right) \\ &+ \frac{1}{2}a^2\left(8 + n^2\pi^2 - \frac{2(24 + 5n^2\pi^2)}{\alpha} + \frac{24(8 + n^2\pi^2)}{\alpha^2}\right). \end{aligned} \tag{3}$$

In Supplementary Information, we compare this result to the exact numerical Bokaian calculation[35] valid for ideal clamping ($\alpha \to \infty$). For $a < 0.1$ the agreement is very good, but degrades with increasing n, demonstrating that higher orders need to be taken into account in the Taylor a-expansion. Note the difference between Eq. (34) and expressions that can be found in the literature.[10,24]

Experimental data and theory are compared in Fig. 2. On the left panel, we present the expected f_0 scalings with $1/L$ (inverse length) and n (mode number; in the normalized plot, $f_0(n)/f_{n,0}$ is at first order a constant). However on the right panel, we demonstrate how the width w of the beam influences the resonance frequencies: $f_0(n = 1)/f_{n=1,0}$ *decreases* with increasing width, independently of length L. This is rather surprising (since f_0 is independent of w in the high-stress limit of Euler-Bernoulli theory), and the effect is less pronounced for higher n (inset left panel). Inspecting Eq. (34), we see that this behavior can be obtained

by a simple ansatz on the clamp parameter α:

$$\alpha \propto \frac{n\pi}{w}, \tag{4}$$

using the simplest guess. This actually means that the anchor becomes *more stiff at higher frequencies, and for smaller beam widths.* Eq. (4) is fit on data, see lines in Fig. 2, demonstrating very good agreement. The extracted parameter is characteristic of our clamp geometry, especially its length L_c. How the resonance frequency of cantilevers decreases with increasing L_c had been investigated numerically in Refs.[31,36] Here, our approach is to fit this dependence by an effective spring constant α; see Supplementary Information for quantitative parameters, and discussion in the Conclusion Section.

We now bring our attention to the quality factor Q, or equivalently the damping parameter $\Delta f = f_0/Q$. We remind that for our devices, radiation loss can be safely neglected.[24] Beyond the nanomechanics literature which clearly established that friction is directly related to bending,[11,12] we shall discuss internal damping from a *materials science* perspective. An ideal solid described in continuum mechanics obeys elasticity theory:[13] one introduces strain and stress tensors which are related linearly by two elastic constants (for isotropic materials), e.g. Young's modulus E and Poisson's ratio ν. When friction mechanisms take place, deviations from this "Hookean" behavior appear: the solid is called *anelastic*. This essentially means that one has to introduce a non-conservative force which acts upon each elementary volume $\delta\tau$ of the material. The most natural modeling consists in introducing the rates of change of strain and stress tensors in the elastic equations, while keeping the hypothesis of linearity.[37]

The simplest such linear superposition is the *Zener model*,[37] and it describes rather well low-frequency (kHz) elastic properties of conventional materials (like metals) probed by Dynamic Mechanical Analysis (DMA). More complex models can be analyzed in order to reproduce the behavior of other materials, or higher frequencies measurements. Their

implication is essentially to generate a frequency-dependent Young's modulus $E(f)$ and friction term proportional to the rate of change of the stress tensor, which can thus be interpreted as an effective viscosity $\eta(f)$. As for the elastic constants, when introducing viscosity in a fluid one has to define (in the simplest case) *two* constants: η and ζ the second viscosity.[38] For the sake of simplicity, in our case we will use the same parametrization as for the elastic properties and we introduce a damping modulus E_p with a damping Poisson's ratio ν_p (which are both also functions of frequency). As a consequence, when solving for a harmonic motion using complex forms, linear friction is *equivalent to replacing* Young's modulus by a complex Young's modulus[37] $E \to E + iE_2$: the linear mechanical response is de-phased from the excitation. This is a fairly simple writing which is widely used,[11,12] but the price to pay is that all details of the friction model are hidden within the constant $E_2(f)$. Especially, its frequency-dependence (from first principles E_2 is function of f) is an important ingredient for the understanding of microscopic processes at stake. The complete mathematical analysis can be found in Supplementary Information.

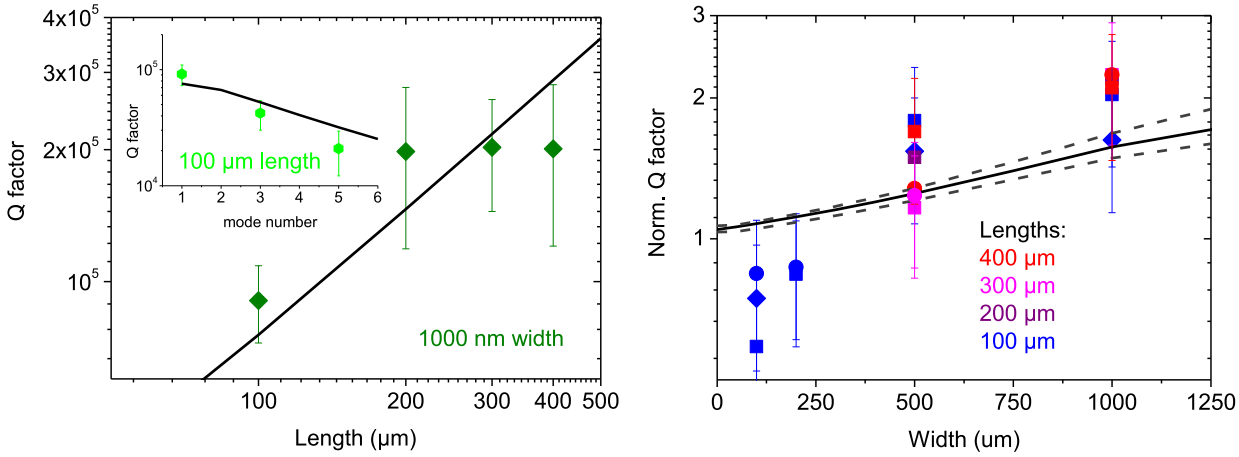

Figure 3: Left, main: dependence of quality factor on length L for the first flexure $n = 1$ (all devices having $w = 1000$ nm). Left, inset: quality factor of 100 μm long device as a function of mode number n. Right: Q normalized to the extrapolated value at $w \to 0$ for mode $n = 1$ of all devices, as a function of width w. The lines correspond to Eqs. (5,6,44) using a simple ansatz for the clamp parameter α, see text.

The quality factor Q writes, for any mode n:

$$Q(n,a,\alpha) = Q_{n,0}\,\frac{P_f(n,a,\alpha)^2}{P_Q(n,a,\alpha)}, \tag{5}$$

with $Q_{n,0} = f_{n,0}^2/(f_{n,0}\Delta f_{n,0})$ the usual n^{th} mode quality factor with:

$$f_{n,0}\Delta f_{n,0} = \frac{n^2}{4\sqrt{3}}\,\frac{e}{L^3}\left(\frac{E_2}{\rho\sqrt{E/\sigma}}\right). \tag{6}$$

Eq. (6) has a single material-dependent fit parameter: E_2 (ρ, E and σ being known from resonance frequency fits). The P_Q function is obtained as:

$$\begin{aligned} P_Q(n,a,\alpha) &= 1 - \frac{6}{\alpha} + \frac{24 - n^2\pi^2}{\alpha^2} \\ &+ a\left(6 + \frac{1}{2}n^2\pi^2 - \frac{48 + 6n^2\pi^2}{\alpha} + \frac{144 - 8n^2\pi^2}{\alpha^2}\right). \end{aligned} \tag{7}$$

For ideal clamping ($\alpha \to \infty$), it is found experimentally that Q scales linearly with L,[11] and falls with increasing thickness (roughly as $1/e$ in Ref.[23]) and mode number n.[11] This has been fit with E_2 essentially frequency-independent;[11,12] we reproduce this result in Supplementary Information by fitting the numerical solutions from Ref.[11] Note the difference between Eqs. (5,6,44) and the expressions derived for membranes.[12,24]

Our data and theory are presented in Fig. 3. On the left panel, we show the conventional dependencies in L and n (the line is calculated with a fit E_2 value, see Supplementary Information). On the right panel, we demonstrate the soft clamping generated by our simple design: Q grows substantially with increasing width w. The dashed upper curve is calculated for 100 μm length, the lower one for 400 μm and the full line for 200 μm length. The clamp parameter α used here is *the same one* as for Fig. 2. The agreement is relatively good, but the remarkable result is that we predict theoretically the right tendency: the clamp degree of freedom reduces the bending at the anchor, which increases the Q. Introducing a boundary torsion spring $\gamma_l = \gamma_r = \gamma$ increases even further the effect; however, fitted values

demonstrate that one requires a higher order expansion than the order 2 in torque for the quantitative result to be valid. We therefore preferred to keep this aspect outside of the present discussion.

Conclusion

We report on experiments performed on flexural nano-mechanical doubly-clamped beams, subject to an axial force load. We demonstrate that their suspended anchoring points act as an "easy soft clamping": it is responsible for both a downward resonance frequency shift and an increase in quality factor. We present an analytic theory that fits the data, based on simple boundary conditions: forces and torques undergone by the beam's ends, and due to the suspended clamp. It turns out that the effective clamp spring constants $k_{l,r}$ are the dominant ingredient (with l, r standing for left and right). For symmetric devices with similar clamps, $k_{l,r} \approx k$ is found to be $k \propto f/w$, with f frequency and w beam width. For the frequency shift, following Ref.[31] this can be recast in an effective lengthening $L \to L + \Delta L$ with $\Delta L \propto w/f$ at lowest order (and clamp-parameter dependent). For the quality factor, the fit is reasonably good but could be improved with a torque spring parameter $\Gamma_{l,r}$. To do so, the theory would need to be improved; likewise, it could be extended to the case of beams with no (or very little) axial stress, and even to cantilevers. The problem addressed here is extremely widespread, and beams with a "natural" clamp undercut (i.e. due to the fabrication process) are extensively used. For this reason, we believe that our work is very relevant to nano-mechanical design, for both defining precisely resonance frequencies (mandatory when multiplexing is at hand) and quality factors.

Author Information

Corresponding Author

*: Eddy Collin, eddy.collin@neel.cnrs.fr.

Notes

The authors declare no competing financial interest.

Data Availability: the data that support the findings of this study are openly available in **Cloud Néel** at https://cloud.neel.cnrs.fr/index.php/s/CnnYPKn8XHYZgXa, reference number.[39]

Acknowledgement

We acknowledge the use of the Néel facility *Nanofab* for the devices fabrication, and the Néel *Cryogenics* facility for help with the low temperature setup. The authors acknowledge support from the ERC CoG grant ULT-NEMS No. 647917, and ERC StG grant UNIGLASS No. 714692. The research leading to these results has received funding from the European Union's Horizon 2020 Research and Innovation Programme, under grant agreement No. 824109, the European Microkelvin Platform (EMP).

Supporting Information Available

Supplementary Information document: provides details about the samples, and the complete description of the mathematical modeling. The analytic theory (derived using Mathematica®) is compared to published theoretical results with ideal clamping conditions. Numerical finite element simulations (COMSOL®) are also presented, reproducing qualitatively the data.

Modal expansion

We start by presenting the theoretical modeling. We consider the case of thin-and-long beams, i.e. $w \ll L$ and $e \ll L$ (w width, e thickness and L length).

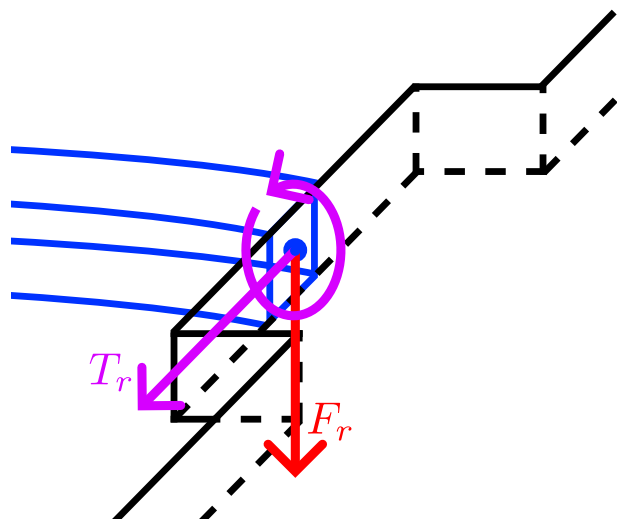

Figure 4: Schematic of (right) clamp with force F_r and torque T_r that the suspended part (black) exerts on the beam (in blue, see text).

From the well-known Euler-Bernoulli equation (including both bending and stress terms), we describe the flexure $f(z,t)$:

$$EI_z \frac{\partial^4 f(z,t)}{\partial z^4} - S\frac{\partial^2 f(z,t)}{\partial z^2} = -\rho A \frac{\partial^2 f(z,t)}{\partial t^2} \tag{8}$$

where $A = we$ - cross-section area, $I_z = \frac{1}{12}we^3$ - second moment of area, E - material's Young's modulus, S - inside tensile ($S > 0$) force of the material, ρ - material density.

We are looking for solution as $f(z,t) = \psi_n(z)x_n(t)$, where $x_n(t) = x_0 \cos(\omega_n t + \varphi)$ is the temporal harmonic part (out-of-plane motion amplitude) and $\psi_n(z)$ - n's mode shape. ω_n is the mode resonance frequency.

On each side, we introduce a force $F_{l,r}$ and torque $T_{l,r}$, see Fig. 4. The relaxed boundary conditions with added spring constant $k_{l,r}$ and inertia $m_{l,r}$ write, for the left l and right r clamps (and similarly for the torques):

Forces:

$$F_l = +EI_z \frac{\partial^3 f(z=0,t)}{\partial z^3} - S\frac{\partial f(z=0,t)}{\partial z} = -k_l f(z=0,t) + m_l \frac{\partial^2 f(z=0,t)}{\partial t^2} \tag{9}$$

$$F_r = -EI_z \frac{\partial^3 f(z=L,t)}{\partial z^3} + S\frac{\partial f(z=L,t)}{\partial z} = -k_r f(z=L,t) + m_r \frac{\partial^2 f(z=L,t)}{\partial t^2} \tag{10}$$

Torques:

$$T_l = -EI_z \frac{\partial^2 f(z=0,t)}{\partial z^2} = -\Gamma_l \frac{\partial f(z=0,t)}{\partial z} + \mathcal{M}_l \frac{\partial^3 f(z=0,t)}{\partial t^2 \partial z} \tag{11}$$

$$T_r = +EI_z \frac{\partial^2 f(z=L,t)}{\partial z^2} = -\Gamma_r \frac{\partial f(z=L,t)}{\partial z} + \mathcal{M}_r \frac{\partial^3 f(z=L,t)}{\partial t^2 \partial z} \tag{12}$$

Note signs in forces and torques definition.

The general solution writes as:

$$\begin{aligned}\psi_n(z) = C_{n,1} \sin\left(k_{n+}\frac{z}{L}\right) + C_{n,2}\cos\left(k_{n+}\frac{z}{L}\right) \\ + C_{n,3}\sinh\left(k_{n-}\frac{z}{L}\right) + C_{n,4}\cosh\left(k_{n-}\frac{z}{L}\right)\end{aligned} \tag{13}$$

Considering a shape normalised to 1: $max[\psi(z)] = 1$ at $z = z_{max}$ (we chose $0 < z_{max} \leq L/2$ with no loss of generality).

Now we expand in the high-stress limit, which means having a small parameter $a = \sqrt{\frac{EI_Z}{SL^2}} \ll 1$:

$$\omega_n = \frac{k_n(a)}{L}\sqrt{\frac{\sigma}{\rho}} \tag{14}$$

where the stress is defined as $\sigma = S/A$.

k_{n-} and k_{n+} are deduced from $k_n(a)$ and they all can be written as Taylor expansions:

$$k_n(a) = k_n(0) + k_n'(0) \cdot a + (1/2)k_n''(0) \cdot a^2 + \dots \tag{15}$$

$$k_{n+}(a) = k_n(0) + k_n'(0) \cdot a + (1/2)[k_n''(0) - k_n^3(0)] \cdot a^2 + \dots \tag{16}$$

$$k_{n-}(a) = 1/a + (1/2)k_n^2(0) \cdot a + [k_n(0)k_n'(0)] \cdot a^2 + \dots \tag{17}$$

Note the $1/a$ in the last Eq. which diverges for small a. In the cosh and sinh functions, it should be treated with care: we shall neglect $\exp(-X)$ terms with $X \propto 1/a$ (what we call exponential approximation), and after take series expansions in a (to lowest order up to a^2). Note that the first order terms goes as a, while the low-stress equivalent expansion leads to small term $1/a^2 = SL^2/(EI_z)$. An equivalent modeling can be performed in this limit, but is outside of the scope of the paper.

Solving the problem produces the mode shape with the definition of constants $C_{n,i}$ and z_{max}, with $k_n(0), k_n'(0), k_n''(0)$. This is performed using an extensive Mathematica® code.

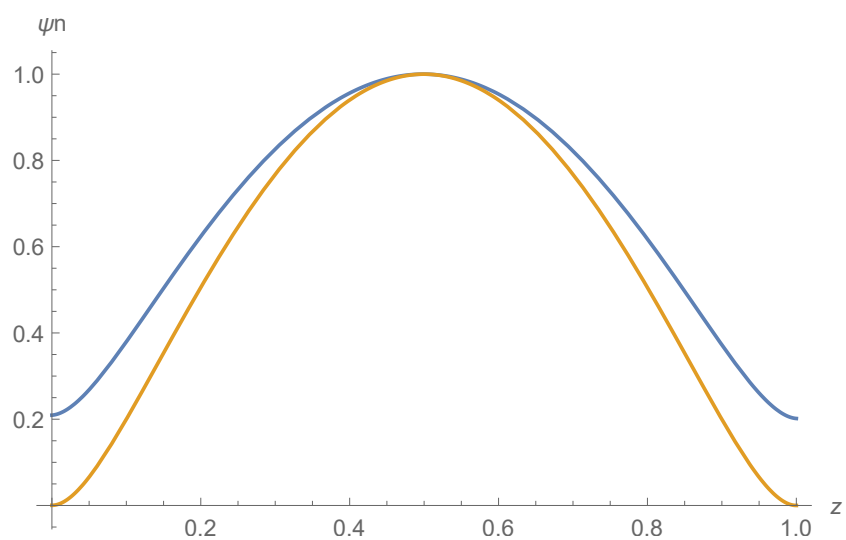

Figure 5: Mode shape with ideal clamping in orange, and with $\alpha_l = \alpha_r = 15.$, $\gamma_l = \gamma_r = 1.$ in blue (see text; in this case, $z_{max} = L/2$ in both cases). For this graphics, $a = 0.05$ and the a expansion has been pushed to order 4 for the ideal clamping terms.

Regrouping restoring forces and inertial components, we fit with for each side two fit

parameters:

$$k_{r,l} \;\rightarrow\; k_{r,l} + m_{r,l}\,\omega^2 \tag{18}$$

$$\Gamma_{r,l} \;\rightarrow\; \Gamma_{r,l} + \mathcal{M}_{r,l}\,\omega^2 \tag{19}$$

without losses of generality. Introducing dimensionless parameters, $k_{r,l} = \frac{S}{L}\alpha_{r,l}$ and $\Gamma_{r,l} = (SL)\,\gamma_{r,l}$. The solutions in the following Sections are given with an expansion at order 2 in $1/\alpha_{r,l} \ll 1$ and $1/\gamma_{r,l} \ll 1$. As an example, we show in Fig. 5 the ideal shape with perfect clamping ($\alpha_{l,r}$ and $\gamma_{l,r}$ being ∞), and the one obtained for imperfect clamps (see caption). The shape is not zero anymore at both ends $z = 0, L$, and (more subtle) the angle $\partial f/\partial z$ is not either.

Stored energy

Defining energies from forces (and force densities):

$$F_{flex} = +EI_z\frac{\partial^3 f}{\partial z^3} \longrightarrow \frac{\partial F}{\partial z} = +EI_z\frac{\partial^4 f}{\partial z^4} \longrightarrow \mathcal{E}_{flex} = \frac{1}{2}EI_z\int_0^L\left(\frac{\partial^4 f}{\partial z^4}f\right)dz \tag{20}$$

$$F_{tens} = -S\frac{\partial f}{\partial z} \longrightarrow \frac{\partial F}{\partial z} = -S\frac{\partial^2 f}{\partial z^2} \longrightarrow \mathcal{E}_{tensile} = \frac{1}{2}S\int_0^L\left(-\frac{\partial^2 f}{\partial z^2}f\right)dz \tag{21}$$

$$\rho A\frac{\partial^2 f}{\partial t^2} \longrightarrow \mathcal{E}_{kin} = \frac{1}{2}\rho A\int_0^L\left(\frac{\partial f}{\partial t}\right)^2 dz \tag{22}$$

Now from integration by parts for flexural energy:

$$\left(\frac{\partial^2 f}{\partial z^2}\cdot\frac{\partial f}{\partial z}\right)' = \frac{\partial^3 f}{\partial z^3}\cdot\frac{\partial f}{\partial z} + \left(\frac{\partial^2 f}{\partial z^2}\right)^2 \tag{23}$$

$$\left(\frac{\partial^3 f}{\partial z^3}\cdot f\right)' = \frac{\partial^4 f}{\partial z^4}\cdot f + \frac{\partial^3 f}{\partial z^3}\cdot\frac{\partial f}{\partial z} \tag{24}$$

From which follows:

$$\frac{\partial^4 f}{\partial z^4} \cdot f = \left(\frac{\partial^3 f}{\partial z^3} \cdot f - \frac{\partial^2 f}{\partial z^2} \cdot \frac{\partial f}{\partial z} \right)' + \left(\frac{\partial^2 f}{\partial z^2} \right)^2 \tag{25}$$

$$\int_0^L \frac{\partial^4 f}{\partial z^4} \cdot f \; dz = \underbrace{\left[\frac{\partial^3 f}{\partial z^3} \cdot f - \frac{\partial^2 f}{\partial z^2} \cdot \frac{\partial f}{\partial z} \right]_0^L}_{\text{boundary term}} + \underbrace{\int_0^L \left(\frac{\partial^2 f}{\partial z^2} \right)^2 \; dz}_{\textit{bulk term}} \tag{26}$$

Same for tensile energy:

$$\left(\frac{\partial f}{\partial z} \cdot f \right)' = \frac{\partial^2 f}{\partial z^2} \cdot f + \left(\frac{\partial f}{\partial z} \right)^2 \tag{27}$$

$$\frac{\partial^2 f}{\partial z^2} \cdot f = \left(\frac{\partial f}{\partial z} \cdot f \right)' + \left[- \left(\frac{\partial f}{\partial z} \right)^2 \right] \tag{28}$$

$$\int_0^L \left(-\frac{\partial^2 f}{\partial z^2} \cdot f \right) \; dz = \underbrace{\left[-\frac{\partial f}{\partial z} \cdot f \right]_0^L}_{\textit{boundary term}} + \underbrace{\int_0^L \left(\frac{\partial f}{\partial z} \right)^2 \; dz}_{\textit{bulk term}} \tag{29}$$

We therefore can define a bulk term and a boundary term for these energies. The boundary term should be $= 0$ for an ideal clamp, i.e. $f = 0$ and $\partial f / \partial z = 0$ at $z = 0, L$. But here, it is not the case; we define for each side:

$$\begin{aligned} \mathcal{E}_{flex,bound} = &+ \frac{EI_z}{2} \frac{\partial^3 f(z=0,t)}{\partial z^3} f(z=0,t) \\ &- \frac{EI_z}{2} \frac{\partial^2 f(z=0,t)}{\partial z^2} \frac{\partial f(z=0,t)}{\partial z} \end{aligned} \tag{30}$$

$$\mathcal{E}_{tens,bound} = - \frac{S}{2} \frac{\partial f(z=0,t)}{\partial z} f(z=0,t) \tag{31}$$

and same for $z = L$, but with reversed signs. One has to pay attention to signs with the definitions and the integration by parts procedure.

Then we define effective energies for the mode, as a function of the mode amplitude x_n:

$$\mathcal{E}_{flex} + \mathcal{E}_{tens} = \frac{1}{2} k_n x_n^2(t) \tag{32}$$

$$\mathcal{E}_{kin} = \frac{1}{2} m_n \dot{x}_n^2(t) \tag{33}$$

Which include in $\mathcal{E}_{flex}$ and $\mathcal{E}_{tens}$ the bulk and boundary terms. One should obviously recover $\omega_n^2 = k_n/m_n$, where k_n is the mode's spring constant and m_n the mode's effective mass per definition, computed from the mode shape ψ_n. This has been explicitly checked in the Mathematica® code. In the literature, this is usually not mentioned.

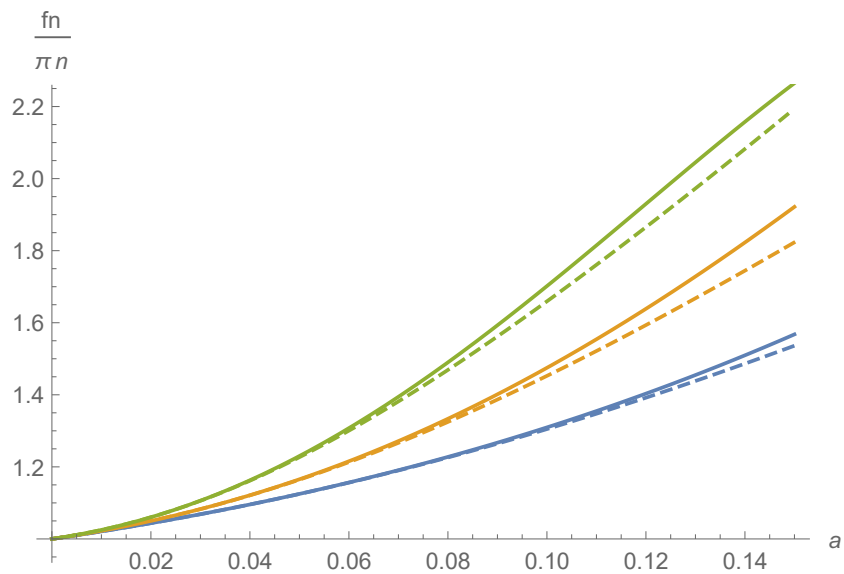

Figure 6: Comparison in the ideal clamp limit of frequency expansion (full lines) to the exact numerical result by [Bokaian, J. Sound and Vibr. **142**, 481 (1990)] (dashed lines). Blue $n = 1$, orange $n = 2$ and green $n = 3$, as a function of a (see text).

In the first place, the modeling allows us to compute the resonance frequencies. The full expression at second order in all parameters reads, for the deviation function P_f introduced in the core of the paper:

$$
\begin{aligned}
P_f(n,a,\alpha) &= 1-\left(\frac{1}{\alpha_l}+\frac{1}{\alpha_r}\right)+\left(\frac{1}{\alpha_l}+\frac{1}{\alpha_r}\right)^2 \\
&+a\left[2-4\left(\frac{1}{\alpha_l}+\frac{1}{\alpha_r}\right)+\left(\frac{6-n^2\pi^2}{\alpha_l^2}+\frac{6-n^2\pi^2}{\alpha_r^2}+\frac{12}{\alpha_l\alpha_r}\right)\right] \\
&+\frac{1}{2}a^2\left[8+n^2\pi^2-(24+5n^2\pi^2)\left(\frac{1}{\alpha_l}+\frac{1}{\alpha_r}\right)\right. \\
&+\left(\frac{48-2n^2\pi^2}{\alpha_l^2}+\frac{48-2n^2\pi^2}{\alpha_r^2}+\frac{96+28n^2\pi^2}{\alpha_l\alpha_r}\right) \\
&\left.-2\left(\frac{1}{\gamma_l}+\frac{1}{\gamma_r}\right)+4\left(\frac{1}{\alpha_l}+\frac{1}{\alpha_r}\right)\left(\frac{1}{\gamma_l}+\frac{1}{\gamma_r}\right)\right]
\end{aligned}
\tag{34}
$$

Note the symmetry $l \leftrightarrow r$ in this expression. A simplified version of it is in the main paper, Eq. (3). In the case of an ideal clamp (effective normalised spring constants $\to \infty$), we compare the expansion to the exact numerical result from [Bokaian, J. Sound and Vibr. **142**, 481 (1990)] in Fig. 6. For the plot, we normalise the frequency to $n\pi$, and take $1/L\sqrt{\sigma/\rho} = 1$. Our computed frequencies match the exact result for typically $a < 0.1$ in the case of ideal clamps, with $n = 1$. And it gets worse for higher modes n, which can be compensated for by taking higher order terms in the a-expansion. For the sake of making a good plot, this is why we used a higher expansion in Fig. 5 (up to fourth order).

Dissipated energy

We shall use the same approach as the one proposed in [Quirin P. Unterreithmeier, Thomas Faust, and Jörg P. Kotthaus PRL **105** 027205 (2010)]. But we formalise it from the continuum mechanics approach as presented in A.N. Cleland, *Foundations of Nanomechanics*, Springer 2003. This implies some minor modification:

- we make it more generic and exact by starting from stress and strain; Poisson's ratios will appear in the expression,
- we start from a proper friction force definition, as in Zener's model, generating a

friction force proportional to the rate of change of the stress. This is what is behind the commonly used complex Young's modulus.

Let us start with the strain 6-component vector for motion of the beam with mode shape $f(z,t)$ and distortion in the $\vec{x}$ direction (see A.N. Cleland 2003):

$$\varepsilon = (\nu x f'', \nu x f'', -x f'', 0, 0, \nu x f''). \tag{35}$$

This expression essentially assumes that planes orthogonal to the neutral axis remain orthogonal to the displaced neutral axis (Euler-Bernoulli approximation), while it guarantees no lateral stresses (see σ_{el} below).

Then the linear response for the stress is:

$$\sigma_{el} = (0, 0, -E x f'', 0, 0, \frac{E\,\nu}{2(1+\nu)} x f'') \tag{36}$$

Where we have both Young's E and Poisson's ν (elasticity theory). We assume linearity to apply, such that this stress adds up to the in-built load σ (purely along $\vec{z}$).

The same linear hypothesis can be made for the local friction stress, which at the macroscopic scale will produce the friction force (prop. to $\dot{x_n}$). But in order to match Zener's low frequency limit, and reproduce a standard viscous friction mechanism, this friction component shall be proportional to the time rate of change of strain $\dot{\varepsilon}$. For the friction component we thus similarly introduce:

$$\begin{aligned}\sigma_{fr} = E_p \cdot \Bigg(& \frac{\nu - \nu_p}{(1+\nu_p)(1-2\nu_p)}, \frac{\nu - \nu_p}{(1+\nu_p)(1-2\nu_p)}, \\ & - \frac{1 - \nu_p - 2\nu\nu_p}{(1+\nu_p)(1-2\nu_p)}, 0, 0, \frac{\nu}{2(1+\nu_p)} \Bigg) \cdot x \dot{f}''\end{aligned} \tag{37}$$

with two parameters describing fricion, E_p and ν_p (similar parametrization of linear response as for stress-strain). Note that the origin of these terms is outside of the scope of the model-

ing; but obviously $E_p(\omega)$ and $\nu_p(\omega)$ depend on frequency, since they originate in microscopic mechanisms which should depend on ω (see comment below).

The power density lost in friction is then:

$$\mathcal{P} = \sigma_{fr} \cdot \dot{\varepsilon} = E_p \left(1 + \frac{\nu^2(5-2\nu_p) - 8\nu\nu_p + 4\nu_p^2}{2(1+\nu_p)(1-2\nu_p)}\right) x^2 \left(\dot{f}''\right)^2 \tag{38}$$
$$= E_p \left(1 + \underbrace{\frac{\nu^2(5-2\nu_p) - 8\nu\nu_p + 4\nu_p^2}{2(1+\nu_p)(1-2\nu_p)}}_{\text{small parameter } o(\nu,\nu_p)}\right) \omega^2 x^2 \left(\frac{\partial^2\psi_n(z)}{\partial z^2}\right)^2 x_n^2(t)$$

Now integration over cross-section $x^2 \to I_z$ and length $\int_0^L$:

$$\iiint \mathcal{P}\ dxdydz = E_p\left[1 + o(\nu,\nu_p)\right]\omega^2 I_z \underbrace{\int_0^L \left(\frac{\partial^2\psi_n}{\partial z^2}\right)^2 dz}_{\text{same integral as in bending energy}} x_n^2(t) \tag{39}$$

In terms of mode definition it can be rewritten introducing the friction force:

$$\iiint \mathcal{P}\ dxdydz = \underbrace{\Lambda_n \dot{x}_n}_{\text{eff. friction force}} \cdot \dot{x}_n = \Lambda_n \omega^2 x_n^2(t) \tag{40}$$

By definition damping parameter $\Delta\omega_n$ is (and $Q = \omega_n/\Delta\omega_n$):

$$\Delta\omega_n = \frac{\Lambda_n}{m_n} \tag{41}$$

Therefore we can identify:

$$\Lambda_n = \underbrace{E_p\left[1 + o(\nu,\nu_p)\right]}_{\text{fit. parameter}} I_z \int_0^L \left(\frac{\partial^2\psi_n}{\partial z^2}\right)^2 dz \tag{42}$$

There is one formal difference here with the [Quirin P. Unterreithmeier, Thomas Faust, and Jörg P. Kotthaus PRL **105** 027205 (2010)] modeling, which uses a compex Young's modulus with imaginary part E_2: their modeling is equivalent to the above one with the

identity $E_p\left[1+o(\nu,\nu_p)\right]=E_2/\omega$. As a result, with $\omega\approx\omega_n$ for a high-Q resonance we have:

$$\omega_n\Delta\omega_n=\frac{e^2E_2}{L^4\rho}\frac{1}{12}\frac{\int_0^1\left(\frac{\partial^2\psi_n[\tilde{z}]}{\partial\tilde{z}^2}\right)^2d\tilde{z}}{\int_0^1\left(\psi_n[\tilde{z}]\right)^2d\tilde{z}} \tag{43}$$

with $\tilde{z}=z/L$. The shape factor defined from ψ_n (the ratio of integrals on the right) tends to $2n^2\pi^2/a$ at lowest order. This leads to the result Eq. (6) of the main paper, written in Hz (here, we have all expressions in Rad/s). From this, one defines the quality factor Q, and then the function P_Q:

$$\begin{aligned}P_Q(n,a,\alpha) &= 1-3\left(\frac{1}{\alpha_l}+\frac{1}{\alpha_r}\right)+\left(\frac{6-\frac{1}{2}n^2\pi^2}{\alpha_l^2}+\frac{6-\frac{1}{2}n^2\pi^2}{\alpha_r^2}+\frac{12}{\alpha_l\alpha_r}\right)\\ &+a\left[6+\frac{n^2\pi^2}{2}-(24+3n^2\pi^2)\left(\frac{1}{\alpha_l}+\frac{1}{\alpha_r}\right)+\left(\frac{60}{\alpha_l^2}+\frac{60}{\alpha_r^2}+\frac{24-8n^2\pi^2}{\alpha_l\alpha_r}\right)\right.\\ &\left.-\left(\frac{1}{\gamma_l}+\frac{1}{\gamma_r}\right)+3\left(\frac{1}{\alpha_l}+\frac{1}{\alpha_r}\right)\left(\frac{1}{\gamma_l}+\frac{1}{\gamma_r}\right)\right]\end{aligned} \tag{44}$$

which represents all deviations from the basic expression (at lowest order in a; note the $l\leftrightarrow r$ symmetry). A simplified version is in the main paper, Eq. (7). In the limit where the clamp spring constants $\alpha_{l,r},\gamma_{l,r}$ tend to ∞, one recovers the usual tendencies: a Q factor that grows as L, and decreases with mode number n. We demonstrate this by comparing our formulas to the numerical results of [Quirin P. Unterreithmeier, Thomas Faust, and Jörg P. Kotthaus PRL **105** 027205 (2010)]. This is done in Fig. 7, see Caption for the used numerical values (we take here a E_2 independent of ω). The agreement is very good; we believe deviations are due to the finite order of the expansion in a.

Further fits of our own data (including the clamp dependence) are discussed in the next Section.

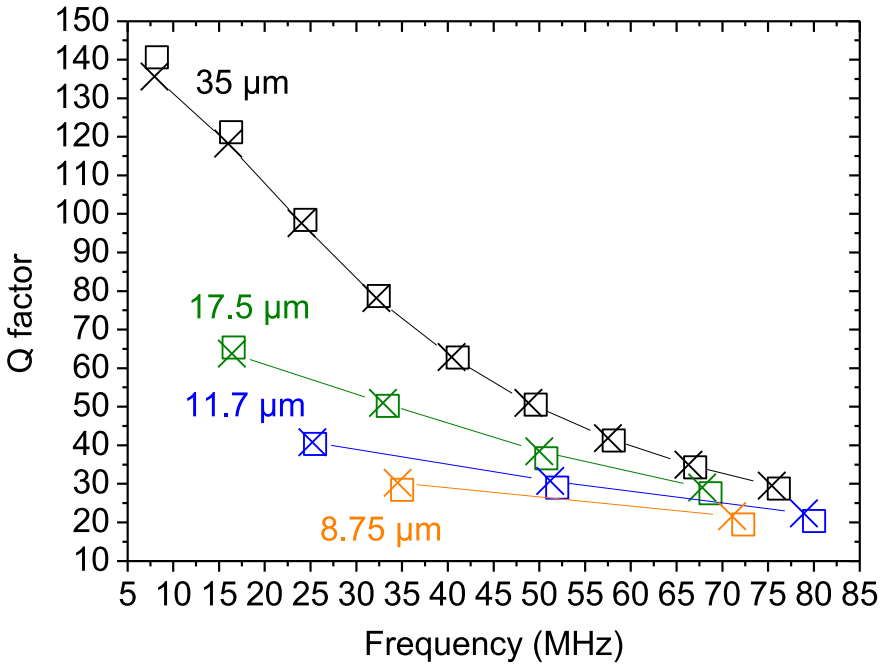

Figure 7: Numerical calculation of Q, f_0 from [Quirin P. Unterreithmeier, Thomas Faust, and Jörg P. Kotthaus PRL **105** 027205 (2010)] (open squares, for different beam lengths L) compared to our analytic solution (crosses), in the case of ideal clamp. Parameters chosen: $\sigma = 0.83$ GPa, $E = 160$ GPa, $\rho = 2800$ kg/m^3, $E_2 = 48$ MPa, $e = 100$ nm, $w = 200$ nm.

Sample Characteristics and clamp fit

The sample fabrication and main characteristics are given in [Golokolenov et al. JLTP 2022]. The measurements have been performed on two chips, on which eight sets of beams (2 groups with the 4 different lengths) were present. Not all of them have been measured (for lack of time), but a good fraction of them has been characterised. Out of all the data acquired, only few data points have been excluded, because they seemed to be out-of-statistics (frequency off by about 20 % max., or Q factor very low and almost independent of parameters w, n). We believe that this comes from the reproducibility of the fabrication, which remains our limiting parameter.

All data in the core of the paper has been fit with a single set of parameters, including a single (symmetric) clamp ansatz. We chose:

- $\sigma = 0.17$ GPa (low-stress sample),
- $\rho = 2800$ kg/m^3,
- $E = 160$ GPa,
- $E_2 = 180$ MPa,

that describe the properties of the bilayer structure. Note that our E_2 is larger than the one of [Quirin P. Unterreithmeier, Thomas Faust, and Jörg P. Kotthaus PRL **105** 027205 (2010)] which had no metal layer. The clamp spring constant is found to be:

$$\alpha_l = \alpha_r = \alpha \approx 2500.\frac{n\pi}{w}, \tag{45}$$

in order to reproduce the properties measured (see discussion in main paper). We verify $\alpha \gg 1$ in the whole range studied. For the sake of completeness, we also included a torque spring, following the same ansatz. However, we realised that in order to influence the fit, this one had to be particularly small, i.e. out of the validity range of the expansion. We therefore preferred not to discuss this point further in the paper; because it would require a more exact expansion to be included. Technically, the graphs of the paper are obtained with:

$$\gamma_l = \gamma_r = \gamma \approx 300.\frac{n\pi}{w}, \tag{46}$$

which has an almost invisible impact on fits (and becomes ~ 1 at worst). This gives us a sort of estimate of the limit within which torques can be neglected.

Eqs. (45,46) are characteristics of the clamp. Within our geometry, its thickness is constant, its composition is the same as for the beam, and we assume that its width W does not matter either, since $w \ll W$ (at worst about 20 μm): for the distortion of the anchoring point, the width of the clamp is essentially infinite. But the length L_c of the suspended part should obviously matter; we give in Tab. 1 the statistics of the clamp's suspended region, for all samples. On average, we have $L_c \approx 12$ μm, within about ± 50 % scatter in

Table 1: Clamp suspension length L_c statistics.

Sample name	left clamp (μm)	right clamp (μm)	mean (μm)
S2 100 μm assym.	3.85	13.1	8.5
S2 100 μm sym.	7.7	11.55	9.6
S2 300 μm	10.	14.	12.
S2 400 μm	5.8	13.5	9.6
S6 100 μm	12.5	16.7	14.6
S6 200 μm	10.8	12.3	11.5
S6 300 μm	13.1	16.9	15.
S6 400 μm	11.3	16.2	13.7

the fabrication. We believe that this scatter could also contribute to the dispersion in the measured properties.

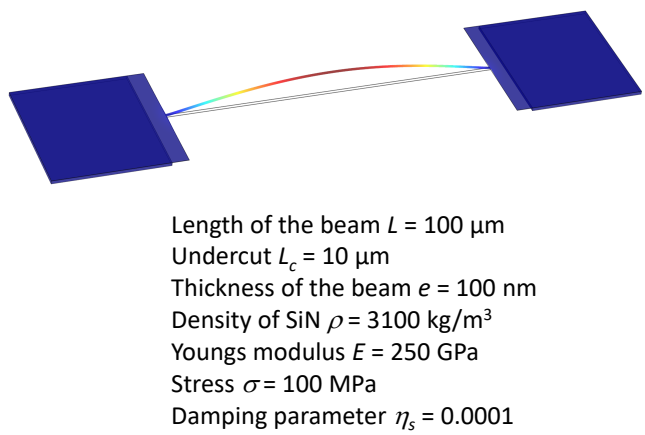

Figure 8: COMSOL® simulation (first $n = 1$ flexure) reproducing the "easy soft clamping" effect (see text). Parameters used for simulation given in Figure.

Comparison to Numerical Simulations

The measured properties can also be qualitatively reproduced by a numerical simulation, demonstrating the "easy soft clamping" effect. To demonstrate this, we perform a simple finite element study on COMSOL®, as shown in Fig. 8. Parameters used given in the figure, except for width w which is varied.

The calculated resonance frequencies f_0 and quality factors Q are presented (in normalised from) in Fig. 9, as a function of w. The very same trend as in the experimental data is visible: the frequency drops with increasing w, while the quality factor grows. It can be fit by a second order polynomial in w, as expected from our analytic theory. The magnitude of the effect is also correct as compared to experiments, but is not in perfect quantitative agreement. We believe that this is due to the exact, and rather precise, choice of parameters that one has to perform to match simulations on data.

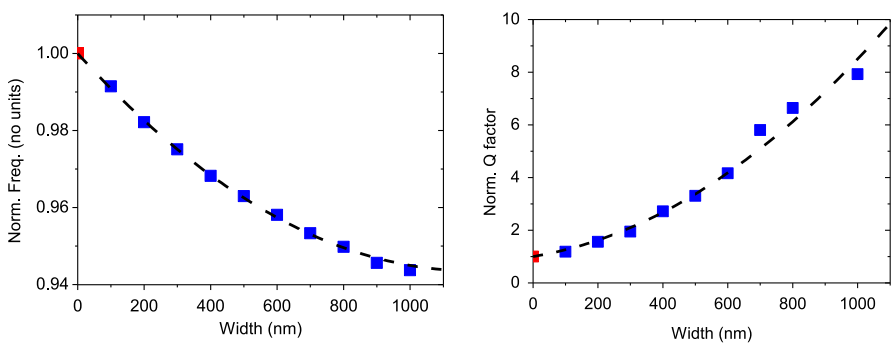

Figure 9: Normalised frequency (left) and quality factor (right) as a function of beam width. The red point is the $w = 0$ extrapolated value, and the dashed lines simple polynomial (second order) fits (see text).

References

(1) Sage, E.; Sansa, M.; Fostner, S.; Defoort, M.; Marc Gély, A. K. N.; Morel, R.; Duraffourg, L.; Roukes, M. L.; Alava, T.; Jourdan, G.; Colinet, E.; Masselon, C.; Brenac, A.; Hentz, S. Single-particle mass spectrometry with arrays of frequency-addressed nanomechanical resonators. *Nat. Comm.* **2018**, *9*, 3283.

(2) Barzanjeh, S.; Wulf, M.; Peruzzo, M.; Kalaee, M.; Dieterle, P.; Painter, O.; Fink, J. Mechanical on-chip microwave circulator. *Nat. Comm.* **2017**, *8*, 953.

(3) Verbridge, S. S.; Parpia, J. M.; Reichenbach, R. B.; Bellan, L. M.; Craighead, H. G.

High quality factor resonance at room temperature with nanostrings under high tensile stress. *J. of Appl. Phys.* **2006**, *99*, 124304.

(4) Verbridge, S. S.; Shapiro, D. F.; Craighead, H. G.; Parpia, J. M. Macroscopic Tuning of Nanomechanics: Substrate Bending for Reversible Control of Frequency and Quality Factor of Nanostring Resonators. *Nano Lett.* **2007**, *7*, 1728.

(5) Fedorov, S. A.; Engelsen, N. J.; Ghadimi, A. H.; Bereyhi, M. J.; Schilling, R.; Wilson, D. J.; Kippenberg, T. J. Generalized dissipation dilution in strained mechanical resonators. *Phys. Rev. B* **2019**, *99*, 054107.

(6) Villanueva, L. G.; Schmid, S. Evidence of surface loss as ubiquitous limiting damping mechanism in SiN micro- and nanomechanical resonators. *Phys. Rev. Lett.* **2014**, *113*, 227201.

(7) Ftouni, H.; Blanc, C.; Tainoff, D.; Fefferman, A. D.; Defoort, M.; Lulla, K. J.; Richard, J.; Collin, E.; Bourgeois, O. Thermal conductivity of silicon nitride membranes is not sensitive to stress. *Phys. Rev. B* **2015**, *92*, 125439.

(8) Defoort, M. *Ph.D.: Non-linear dynamics in nano-electromechanical systems at low temperatures*; Université Grenoble Alpes: Grenoble, 2014.

(9) Hoch, D.; Yao, X.; Poot, M. Geometric tuning of stress in predisplaced silicon nitride resonators. *Nano Lett.* **2022**, *22*, 4013.

(10) Bückle, M.; Klaß, Y. S.; Nägele, F. B.; Braive, R.; Weig, E. M. Universal length dependence of tensile stress in nanomechanical string resonators. *Phys. Rev. Applied* **2021**, *15*, 034063.

(11) Unterreithmeier, Q. P.; Faust, T.; Kotthaus, J. P. Damping of nanomechanical resonators. *Phys. Rev. Lett.* **2010**, *105*, 027205.

(12) Yu, P.-L.; Purdy, T. P.; Regal, C. A. Control of material damping in high-Q membrane microresonators. *Phys. Rev. Lett.* **2012**, *108*, 083603.

(13) Cleland, A. *Foundations of nanomechanics*, 3rd ed.; Springer: Berlin Heidelberg, 2003.

(14) Olkhovets, A.; Parpia, J. M.; Evoy, S.; Carr, D.; Craighead, H. G. Actuation and internal friction of torsional nanomechanical silicon resonators. *J. Vac. Sci. Technol. B* **2000**, *18*, 3549.

(15) Collin, E.; Kofler, J.; Lakhloufi, S.; Pairis, S.; Bunkov, Y. M.; Godfrin, H. Metallic coatings of microelectromechanical structures at low temperatures: Stress, elasticity, and nonlinear dissipation. *J. of Appl. Phys.* **2010**, *107*, 114905.

(16) Hauer, B. D.; Kim, P. H.; Doolin, C.; Souris, F.; Davis, J. P. Two-level system damping in a quasi-one dimensional optomechanical resonator. *Phys. Rev. B* **2018**, *98*, 214303.

(17) Lulla, K. J.; Defoort, M.; Blanc, C.; Bourgeois, O.; Collin, E. Evidence for the role of normal-state electrons in nanoelectromechanical damping mechanisms at very low temperatures. *Phys. Rev. Lett.* **2013**, *110*, 177206.

(18) Maillet, O.; Cattiaux, D.; Zhou, X.; Gazizulin, R. R.; Bourgeois, O.; Fefferman, A. D.; Collin, E. Nanomechanical damping via electron-assisted relaxation of two-level systems. *Phys. Rev. B* **2023**, *107*, 064104.

(19) Photiadis, D. M.; Judge, J. A. Attachment losses of high Q oscillators. *Appl. Phys. Lett.* **2004**, *85*, 482.

(20) Judge, J. A.; Photiadis, D. M.; Vignola, J. F.; Houston, B. H.; Jarzynski, J. Attachment loss of micromechanical and nanomechanical resonators in the limits of thick and thin support structures. *J. of Appl. Phys.* **2007**, *101*, 013521.

(21) Cross, M. C.; Lifshitz, R. Elastic wave transmission at an abrupt junction in a thin

plate with application to heat transport and vibrations in mesoscopic systems. *Phys. Rev. B* **2001**, *64*, 085324.

(22) Wilson-Rae, I. Intrinsic dissipation in nanomechanical resonators due to phonon tunneling. *Phys. Rev. B* **2008**, *77*, 245418.

(23) Schmid, S.; Jensen, K. D.; Nielsen, K. H.; Boisen, A. Damping mechanisms in high-Q micro and nanomechanical string resonators. *Phys. Rev. B* **2011**, *84*, 165307.

(24) Ghadimi, A. H.; Wilson, D. J.; Kippenberg, T. J. Radiation and internal loss engineering of high-stress silicon nitride nanobeams. *Nano Lett.* **2017**, *17*, 3501.

(25) Adiga, V. P.; Ilic, B.; Barton, R. A.; Wilson-Rae, I.; Craighead, H. G.; Parpia, J. M. Approaching intrinsic performance in ultra-thin silicon nitride drum resonators. *J. of Appl. Phys.* **2012**, *112*, 064323.

(26) Tsaturyan, Y.; Barg, A.; Polzik, E. S.; Schliesser, A. Ultracoherent nanomechanical resonators via soft clamping and dissipation dilution. *Nat. Nanotech.* **2017**, *12*, 776.

(27) Yu, P.-L.; Cicak, K.; Kampel, N. S.; Tsaturyan, Y.; Purdy, T. P.; Simmonds, R. W.; Regal, C. A. A phononic bandgap shield for high-Q membrane microresonators. *Appl. Phys. Lett.* **2014**, *104*, 023510.

(28) Suhel, A.; Hauer, B. D.; Biswas, T. S.; Beach, K. S. D.; Davis, J. P. Dissipation mechanisms in thermomechanically driven silicon nitride nanostrings. *Appl. Phys. Lett.* **2012**, *100*, 173111.

(29) Ghadimi, A. H.; Fedorov, S. A.; Engelsen, N. J.; Bereyhi, M. J.; Schilling, R.; Wilson, D. J.; Kippenberg, T. J. Elastic strain engineering for ultralow mechanical dissipation. *Science* **2018**, *360*, 764.

(30) Sadeghi, P.; Tanzer, M.; Christensen, S. L.; Schmid, S. Influence of clamp-widening on

the quality factor of nanomechanical silicon nitride resonators. *J. of Appl. Phys.* **2019**, *126*, 165108.

(31) Babaei Gavan, K.; van der Drift, E. W. J. M.; Venstra, W. J.; Zuiddam, M. R.; van der Zant, H. S. J. Effect of undercut on the resonant behaviour of silicon nitride cantilevers. *J. of Micromech. Microeng.* **2009**, *19*, 035003.

(32) Golokolenov, I.; Alperin, B.; Fernandez, B.; Fefferman, A.; Collin, E. Fully Suspended Nano-beams for Quantum Fluids. *J. of Low Temp. Phys.* **2023**, *210*, 550–561.

(33) Cleland, A.; Roukes, M. External control of dissipation in a nanometer-scale radiofrequency mechanical resonator. *Sensors and Actuators* **1999**, *72*, 256.

(34) Timoshenko, S.; Young, D.; Weaver, W. *Vibrations problems in engineering*, 4th ed.; John Wiley and Sons, 1974.

(35) Bokaian, A. Natural frequencies of beams under tensile axial loads. *J. of Sound and Vibr.* **1990**, *142*, 481.

(36) Sadewasser, S.; Villanueva, G.; Plaza, J. A. Modified atomic force microscopy cantilever design to facilitate access of higher modes of oscillation. *Review of Sci. Instruments* **2006**, *77*, 073703.

(37) Zener, C. *Elasticity and Anelasticity of Metals*, 4th ed.; The University of Chicago Press, 1948.

(38) Landau, L.; Lifshitz, E. *Fluid mechanics*, 2nd ed.; Pergamon Press: Headington Hill Hall, 1987.

(39) Collin, E. Data for Nano beam Clamping Revisited. *Golokolenov2022 Néel* **2022**,